Available online at www.sciencedirect.com
ScienceDirect
Lithos 95 (2007) 279–297
LITHOS
www.elsevier.com/locate/lithos

Forward modeling corona growth in a partially eclogitized leucogabbro, Bourbon Island, North-East Greenland

C. Sartini-Rideout *, J.A. Gilotti, C.T. Foster Jr.

Department of Geoscience, University of Iowa, Iowa City, Iowa, 52242, United States

Received 7 March 2006; accepted 6 August 2006
Available online 22 September 2006

Abstract

Coronitic textures are common in partially eclogitized igneous bodies, such as gabbros, leucogabbros, and anorthosites, east of the Germania Land Deformation Zone in North-East Greenland. Coronas formed by prograde metamorphic processes that transformed the gabbroic bodies to eclogite facies, and record frozen stages of the prograde metamorphic evolution of these rocks. A metaleucogabbro-norite body on Bourbon Island in Jøkelbugt is characterized by three concentric areas: a coronitic core, a mottled inner rim with areas of completely eclogitized material surrounded by a matrix of coronitic metaleucogabbro, and an outer rim of strongly foliated and completely retrogressed amphibolite. The Bourbon body preserves four stages of the prograde metamorphic history: Stage I, Stage II, Stage III, and Eclogite Stage. Stage I coronas are found only in the core of the body, which is the least reacted part of the leucogabbro-norite and the closest to the protolith, and is characterized by the corona sequence Pl_{rim}/Grt+Kfs+Amp/Grt+Amp/Cpx_{rim}. The typical corona sequence for Stage II is Pl_{rim}/Grt+Pl+Zo/Cpx_{rim}/Amp_{rim}. Stage III samples show a Pl_{rim}+Ky+Scp/Grt+Pl+Qtz/Qtz+Pl sequence, with the relict clinopyroxene being replaced in part by microcrystalline aggregates of Cpx+Amp+Pl. The Eclogite Stage shows relict Pl completely replaced by Grt, and the relict Cpx completely replaced by aggregates of Omp+Pl+Kfs+Amp. We tested open-system grain boundary diffusion (OSGBD) theories to model the prograde Stage I symplectitic coronas. The observed ratio of the thickness of the different layers is Pl_{rim}:Grt+Kfs+Amp:Grt+Amp:Cpx_{rim} equal to 3:1.3:0.95:0.5. These ratios are very close to the modeled ones of 2.7:1.1:1:0.5. Furthermore, subtle textural changes within the Grt+Kfs+Amp corona were also reproduced by the model. The model gave us insight into the conditions of the metamorphic system in which the coronas formed. The sequence Pl_{rim}/Grt+Kfs+Amp/Grt+Amp/Cpx_{rim} formed by diffusion driven reactions in an open system involving gain of Fe, K, and Na, and loss of Ca and Mg at the original clinopyroxene–plagioclase boundary. Relative mobilities of the different components within the corona layers were $L_{MgMg} > L_{AlAl} > L_{SiSi} > L_{CaCa} > L_{KK} > L_{FeFe} > L_{NaNa}$. Fluid circulation was active to some degree during the transformation to eclogite. The differences between core, inner rim, and the two domains within the inner rim of the metaleucogabbro-norite can be explained by different degrees of fluid circulation in different portions of the rock. The presence of phases containing Cl and P, such as scapolite, in completely eclogitized samples supports the presence of fluid circulation in the system. Another possible explanation for the mottled appearance of the inner rim is protolith heterogeneity.

Keywords: Coronas; Symplectites; Eclogite; Diffusion modeling; Greenland Caledonides

* Corresponding author.
E-mail address: claudia-sartini@uiowa.edu (C. Sartini-Rideout).

0024-4937/$ - see front matter © 2006 Elsevier B.V. All rights reserved.
doi:10.1016/j.lithos.2006.08.001

1. Introduction

Parts of the structural block east of the Germania Land Deformation zone in the North-East Greenland Eclogite Province (NEGEP) (Fig. 1a) (Gilotti, 1993; Hull and Gilotti, 1994) experienced ultrahigh-pressure metamorphic conditions (Gilotti and Ravna, 2002; McClelland et al., 2006), yet numerous examples of partially eclogitized igneous bodies are preserved within the gneisses (Gilotti and Elvevold, 1998; Lang and Gilotti, 2001).

A common occurrence in partially eclogitized igneous bodies, both in the North-East Greenland Eclogite Province and elsewhere, is the presence of coronitic textures (Mørk, 1985a,b; Indares, 1993; Indares and Dunning, 1997; Gilotti and Elvevold, 1998; Lang and Gilotti, 2001). Coronas indicate textural and mineralogical disequilibrium, and represent frozen stages of the metamorphic history of the rocks in which they form. These frozen stages offer an important opportunity to determine the prograde reaction sequence and the metamorphic history that leads to the formation of eclogites. Corona textures form as a result of a change in P, T and/or f_{H2O}. As a consequence of these changes, mineral phases become locally unstable but can only react along their margins because of slow kinetics.

Some coronas, especially symplectitic ones, are considered to be retrograde textures developed during the cooling stages of igneous intrusions (Ashworth and Birdi, 1990; Ashworth et al., 1992; Ashworth and Sheplev, 1997; Attoh, 1998; Markl et al., 1998). Examples of prograde coronas have been described by Mørk (1985a,b, 1986), Pognante (1985), Indares (1993), Indares and Dunning (1997), Gilotti and Elvevold (1998), and Lang and Gilotti (2001).

Although coronas have been amply described, not much is known about the conditions and metamorphic processes that lead to the formation of coronitic textures, especially in the case of prograde coronas. Modeling of coronas has progressed from Fisher's (1977) early works to more applied studies (Foster, 1990; Ashworth et al., 1992; Ashworth and Sheplev, 1997; Markl et al., 1998). The early studies approached modeling using mass-balance and steady-state diffusion equations to model corona sequences in a closed system, following Joesten

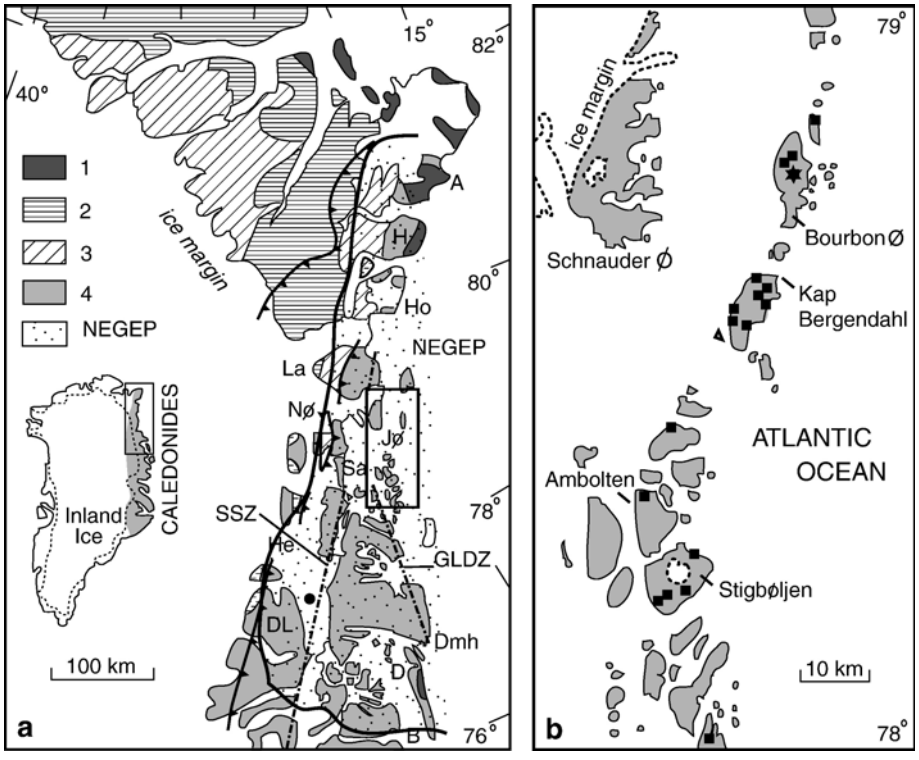

Fig. 1. (a) Geological map of the North-East Greenland Eclogite Province (modified from Gilotti and Elvevold, 1998). Units are: 1. Carboniferous and younger basins; 2. Late Proterozoic to Silurian sedimentary sequences; 3. Mid-Proterozoic sediments and basalt sequences; 4. Precambrian gneisses including eclogite facies rocks; NEGEP: North-East Greenland Eclogite Province; H: Holm Land; Jø: Jøkelbugt; Dmh: Danmarkshavn; D: Dove Bugt; Sa: Sanddal; GLDZ: Germania Land deformation zone; SSZ: Storstrømmen Shear Zone. (b) Map of Jøkelbugt showing the location of Bourbon Island, the Bourbon metaleucogabbro-norite (star), and all the other eclogitized gabbroic bodies (filled squares).

(1977). More recent studies agree that spatially well-organized coronas are not entirely explained by steady-state diffusion in isochemical systems. Joesten's (1977) method has been modified by Ashworth and Birdi (1990) and Johnson and Carlson (1990) to allow for modeling in an open system. Until now modeling has focused on retrograde textures, and not prograde ones.

The goal of this study is to describe the progressive stages of eclogitization preserved in a coronitic leucogabbro-norite and provide insight into the nature of the environment in which such disequilibrium textures formed. Stage I coronas are modeled using non-equilibrium thermodynamics and, in particular, open-system grain boundary diffusion theories (OSGBD) (Ashworth and Birdi, 1990; Ashworth et al., 1992; Ashworth and Sheplev, 1997). This study tests open-system grain boundary diffusion theories and models (Ashworth and Birdi, 1990; Ashworth et al., 1992; Ashworth and Sheplev, 1997) on prograde coronas.

2. Geological setting

The NEGEP (Gilotti, 1993) extends for about 400 km from Holm Land in the north, to Dove Bugt in the south (Fig. 1a). The province is composed of amphibolite-facies quartzofeldspathic orthogneisses derived from 2.0 to 1.8 Ga calcalkaline intrusive complexes and 1.74 granitic intrusions overprinted by Caledonian metamorphism (Kalsbeek et al., 1993; Hull et al., 1994; Kalsbeek, 1995; Brueckner et al., 1998). The orthogneisses contain meter-scale mafic pods with variably preserved eclogite facies assemblages. The eclogite facies rocks include eclogites *sensu stricto*, garnet websterites, garnet clinopyroxenites, coronitic gabbroic intrusions, and websterites (Gilotti, 1994). Protoliths of the eclogite facies rocks were pre-Caledonian mafic dikes, mafic to ultramafic intrusions, and mafic xenoliths in the calcalkaline batholiths (Gilotti, 1993, 1994; Brueckner et al., 1998). The province is divided into three structural blocks by two shear zones: the sinistral Storstrømmen shear zone (Holdsworth and Strachan, 1991) and the dextral Germania Land deformation zone (Hull and Gilotti, 1994) (Fig. 1a). The western and central blocks were metamorphosed under medium-T (600–750 °C), high-P (1.5–2.3 GPa) conditions (Brueckner et al., 1998; Elvevold and Gilotti, 2000) in the Devonian, with the age of HP metamorphism varying between 410–390 Ma (Gilotti et al., 2004). Parts of the eastern block on the other

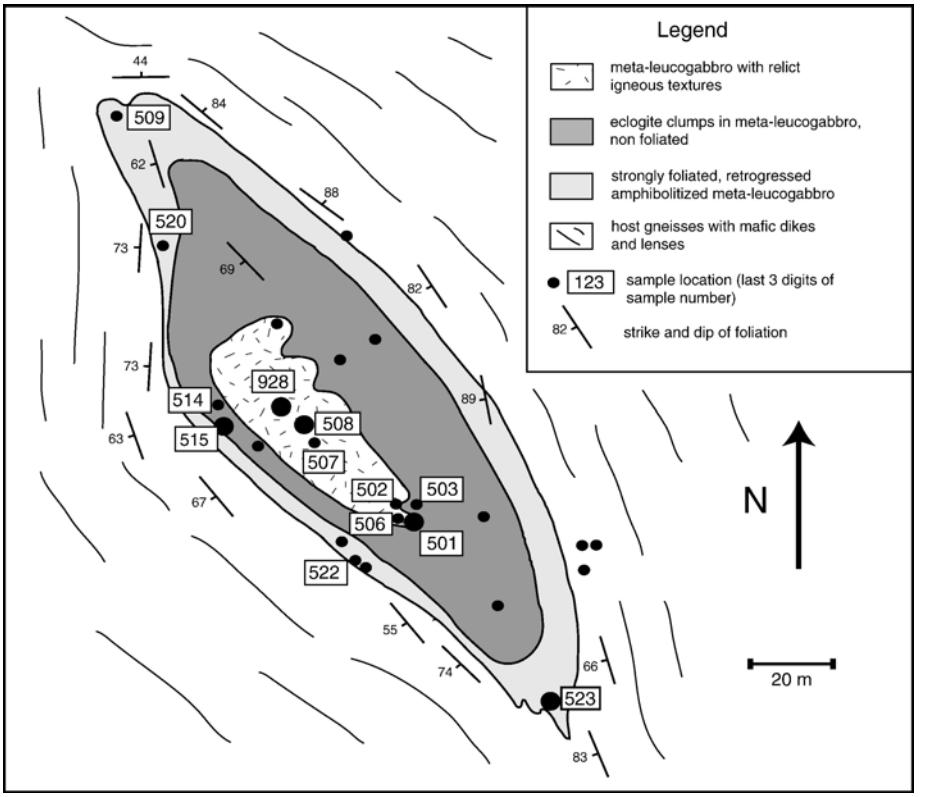

Fig. 2. Detailed geological outcrop map of the metaleucogabbro-norite body on Bourbon Island (modified from Gilotti and Elvevold, 1995) showing sample locations. Numbered samples are described in this study.

Table 1
Whole rock geochemistry for sample 432928

	432928
SiO_2	51.633
TiO_2	0.971
Al_2O_3	17.982
$FeO+Fe_2O_3$	10.134
MnO	0.143
MgO	5.560
CaO	9.931
Na_2O	2.740
K_2O	0.753
P_2O_5	0.202
LOI	0.120
Total	100.169

hand, experienced ultrahigh-pressure (UHP) metamorphism. Coesite is included in zircons from eclogites as well as the host gneisses (McClelland et al., 2006). Thermobarometry on the peak assemblage garnet+omphacite+kyanite+phengite+coesite in kyanite eclogites, gives temperatures above 950 °C at 3.6 GPa (Gilotti and Ravna, 2002). The UHP metamorphism is 360–347 Ma based on $^{206}U/^{238}Pb$ ages from coesite-bearing metamorphic zircons in kyanite eclogites and host gneisses (Gilotti et al., 2004; McClelland et al., 2006).

Many of the partially eclogitized anorthosite and leucogabbro bodies are found between 78° and 79° N in the eastern block, on the islands in Jøkelbugt (Gilotti and Elvevold, 1998) (Fig. 1a and b), although they occur throughout the province as far west as Sanddal (Lang and Gilotti, 2001). These gabbros are thought to be Paleoproterozoic because they display 2.1 Ga Sm–Nd model ages (Stecher and Henriksen, 1994). The bodies were not completely equilibrated to eclogite facies during the Caledonian orogeny, probably because of a combination of factors related to the composition of the protolith, lack of fluid availability, and reaction kinetics (Lang and Gilotti, 2001). Although there is no evidence that these partially eclogitized bodies in the eastern block experienced UHP conditions, the fact that they are only partially eclogitized does not preclude UHP conditions. For example, Zhang and Liou (1997) report coronitic textures in the core adjacent to coesite-bearing eclogitic margins of a metagabbro in the Sulu Terrane of eastern China.

3. Field relations

The studied metaleucogabbro-norite is located on Bourbon Island (Fig. 1b) at UTM 27x WH 558900 m, 8747400 m. The igneous body crops out as a 200 m long by 60 m wide lens surrounded by gray orthogneiss (Fig. 2). The foliation in the gneiss is concordant with the contact. Three distinct concentric areas can be recognized in the metagabbro: an undeformed core, a mottled inner rim and a foliated amphibolite-facies outer rim (Fig. 2). The core of the body is made of undeformed, medium-grained, coronitic leucogabbro-norite (Table 1 and Fig. 3a). The inner rim (5 to 40 m thick)

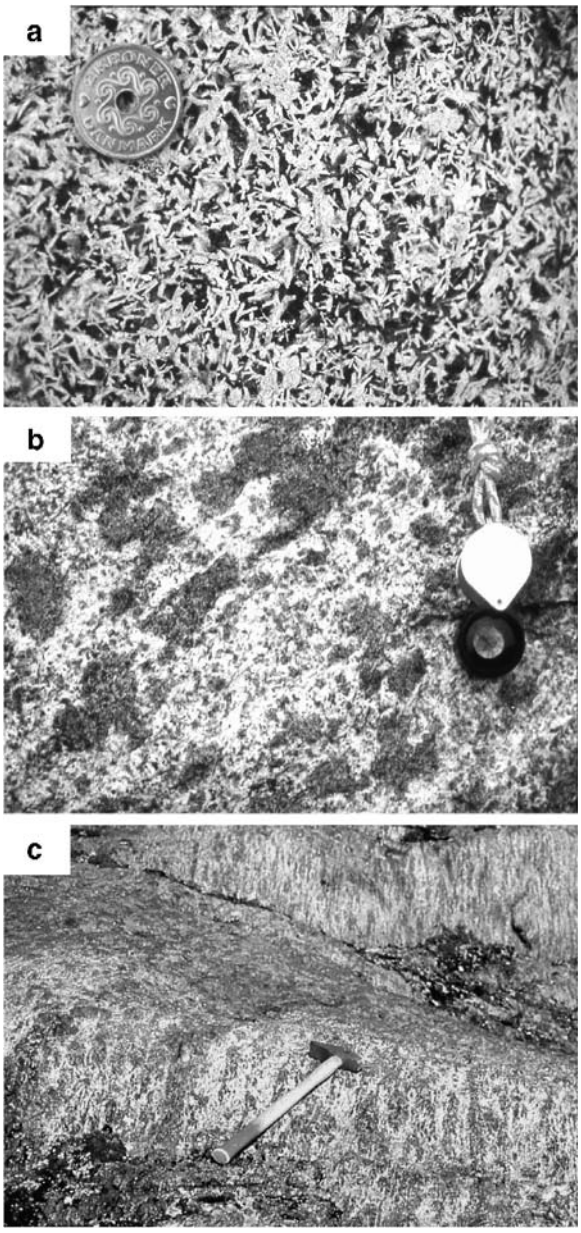

Fig. 3. Outcrop photographs of the three concentric parts of the Bourbon metaleucogabbro-norite. (a) The core of the body is made of leucogabbro with relict sub-ophitic igneous textures. (b) The inner rim contains dark clumps of eclogite within areas of plagioclase-rich coronitic leucogabbros. (c) The outer rim is made of foliated and retrogressed amphibolite-facies material (hammer is 40 cm long).

contains fist-sized clumps of garnet+omphacite surrounded by a plagioclase-rich, coronitic matrix that resembles, at the outcrop scale, the metaleucogabbro-norite core (Fig. 3b). The 5 to 20 m thick outer margin of the body is strongly foliated and retrogressed to amphibolite facies (Fig. 3c). The foliation in the outer rim is concordant with the gneissosity in the surrounding orthogneiss, and strikes about 320°. The transitions among the three zones of the metaleucogabbro-norite are quite sharp and occur over a distance of 20 to 50 cm.

The felsic to intermediate gneisses surrounding the metaleucogabbro-norite contain amphibolite-facies assemblages. A representative mineral assemblage is quartz+plagioclase+garnet+hornblende+biotite±muscovite+epidote/zoisite+rutile±titanite. In addition to the partially eclogitized body described above, the orthogneiss is also host to well-equilibrated eclogite pods.

4. Textures and mineralogy

Different coronitic stages are recognizable within the leucogabbro-norite that record the transformation of the igneous rock to eclogite. In the core of the leucogabbro, the most pristine relict igneous phases and textures are still partially preserved. The core consists mostly of plagioclase and clinopyroxene. Samples from the inner core of the lens have an apparently unaltered igneous texture at the outcrop scale, but reveal coronitic textures

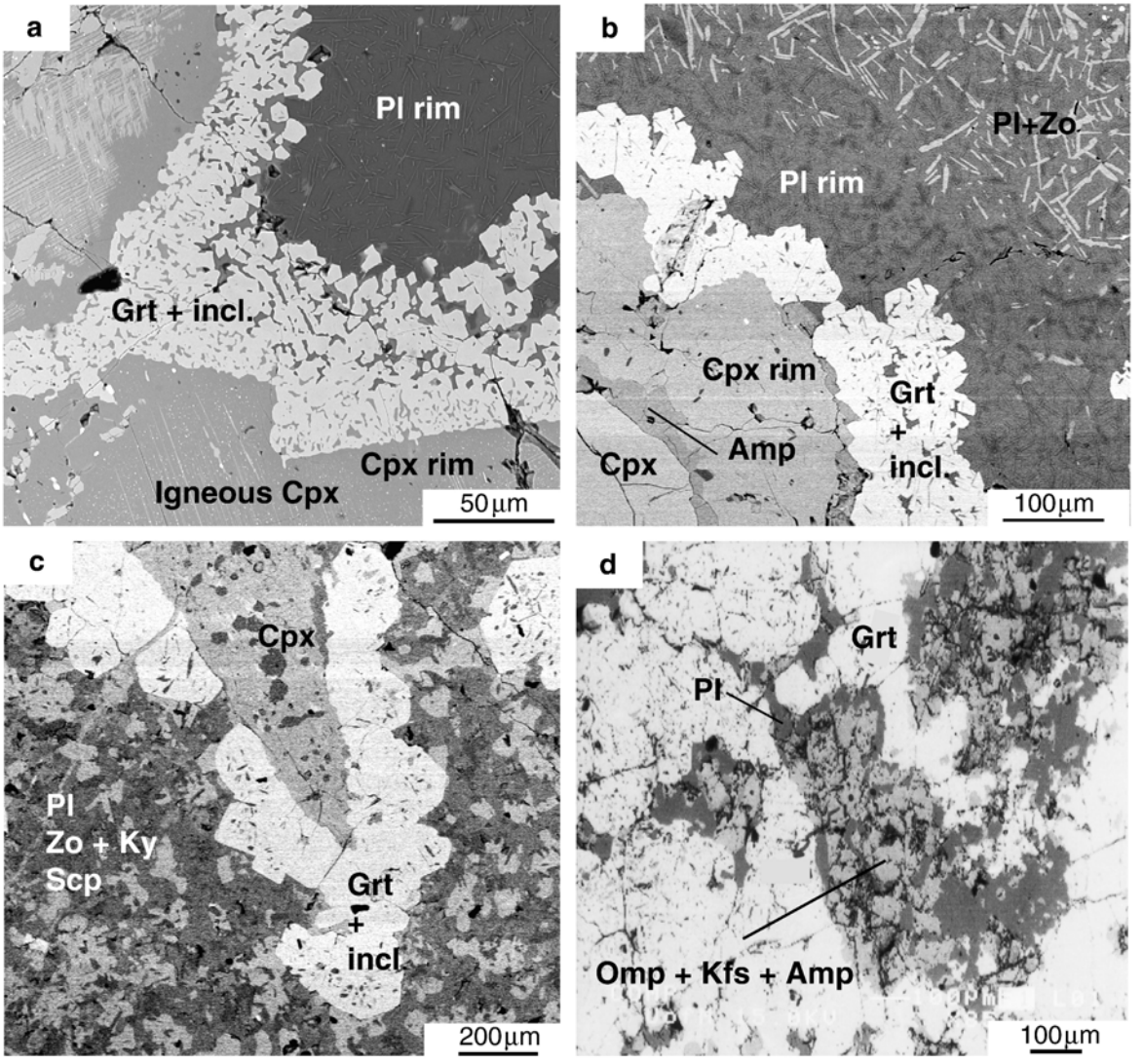

Fig. 4. Backscattered electron images of the different stages of eclogitization recognized in the Bourbon Leucogabbro. (a) Stage I; (b) Stage II; (c) Stage III; (d) Eclogite. Mineral abbreviations from Spear (1993).

Table 2
Mineralogy table showing the location of each sample and its metamorphic stage

Sample #	Location	Stage	Mineralogy
434508	Core	I	Pl+Cpx+Opx+Grt+Zo+Qtz+Amp+Kfs±Bt±Ms+Ttn+oxides
434507	Core	I	Pl+Cpx+Ol+Grt+Zo+Qtz+Opx+Amp±Kfs±Bt+Ttn+oxides
434506	Core	II	Pl+Cpx+Grt+Zo+Qtz+Amp+Kfs+Bt+Ms+oxides
434501	Core	II	Pl+Cpx+Grt+Zo+Qtz+Amp+Kfs+Bt+Ms+oxides
434502	Core	II	Pl+Cpx+Grt+Zo+Qtz+Amp+Kfs+Bt+Ms+oxides
434503	Inner rim	III	Pl+Cpx+Grt+Zo+Ky+Qtz+Amp±Kfs+oxides
434515b	Inner rim	III	Pl+Cpx+Omp+Grt+Zo+Ky+Scp+Qtz±Amp
434514	Inner rim	III	Pl+Cpx+Omp+Grt+Zo+Ky+Scp+Qtz±Amp
434515a	Inner rim	Eclogite	Omp+Grt+Amp+Kfs+Pl
434509	Outer rim	Amphibolite	Amp+Pl+Qtz+Grt+Zo+Ms+Bt+oxides
434520	Outer rim	Amphibolite	Amp+Pl+Qtz+Grt+Zo +Ms+Bt+oxides
434522	Outer rim	Amphibolite	Amp+Pl+Qtz+Grt+Zo+Ms+Bt+oxides
434523	Outer rim	Amphibolite	Amp+Pl+Qtz+Grt+Zo+Ms+Bt+oxides

Pl: plagioclase; Cpx: clinopyroxene; Omp: omphacite; Opx: orthopyroxene; Ol: olivine; Grt: garnet; Zo: zoisite; Ky: kyanite; Qtz: quartz; Amp: amphibole; Kfs: K-feldspar; Bt: biotite; Ms: muscovite; Scp: scapolite; Ttn: titanite.

when observed microscopically (Fig. 4a). The coronas show delicate symplectitic structures in back-scattered electron (BSE) images. Multi-layer coronas form at the contact between clinopyroxene and plagioclase, orthopyroxene and plagioclase, olivine and plagioclase, and titanite and plagioclase. The coronas are thicker in the inner rim of the leucogabbro, where complete eclogitization is observed in patches (Fig. 4c and d). The different metamorphic stages preserved in the Bourbon body are described in detail below. Table 2 presents the minerals and textures in the studied samples. All samples with six digit numbers are part of the GEUS (Geological Survey of Denmark and Greenland) database.

4.1. Stage I

Stage I coronas are found only in the core of the body (e.g. 434508; Figs. 3a and 4a). The undeformed core is the least reacted part of the leucogabbro-norite and, thus, closest to the protolith. Medium grained igneous textures are preserved, with randomly oriented plagioclase laths plus some interstitial olivine grains (found only in sample 434507) and intergranular clinopyroxene plus minor amounts of orthopyroxene (the latter only found in sample 434508).

Small needles of zoisite, formed by the breakdown of plagioclase, cloud the plagioclase crystals. Zoisite needles are abundant in the central parts of the plagioclase crystals (25–30% modal amount), while a zoisite-free (zoisite< 2%) more sodic plagioclase rim (100 to 150 μm thick) is present at the margins of the crystals in contact with clinopyroxene and orthopyroxene (Fig. 4a). The zoisite-free rim has a mottled appearance (Fig. 4a), which we interpret as the replacement of zoisite by plagioclase. No unaltered igneous plagioclase is observed in any of the samples.

The clinopyroxene domains are clouded by exsolved oxides, and show a thin (approximately 201 μm), irregular oxide-free rim of recrystallized diopsidic clinopyroxene, which texturally seems to have grown inward and replaced the more augitic relict crystals (Fig. 4a and layer 4 in Fig. 5).

Garnet crystals start to nucleate at the contact between plagioclase and clinopyroxene, where they form beautiful discontinuous coronas (Fig. 4a). The thickness of the garnet coronas is slightly irregular, averaging between 50 and 100 μm. A few garnets also nucleate within the plagioclase domains. BSE images of the coronas reveal that they are symplectitic and consist of two layers that can be distinguished on the basis of the mineral phases intergrown with garnet (Fig. 5, layers 2 and 3). The inner layer (layer 2) closer to the zoisite-free plagioclase rim is

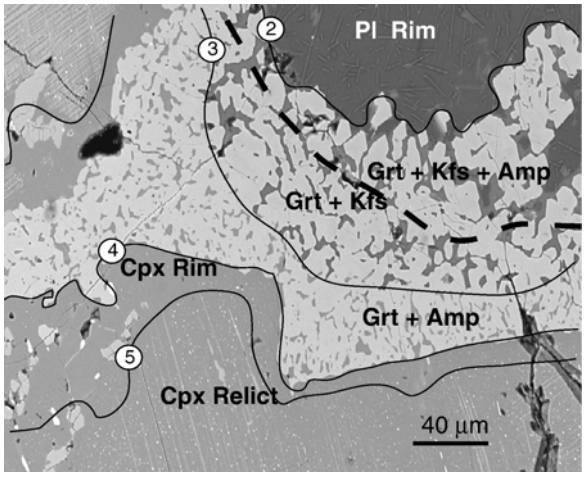

Fig. 5. Back scattered electron image of the Stage I coronitic layers. The continuous lines mark boundaries 2 to 5 that have been entered in the model (compare to Fig. 8), the dashed line marks the boundary within layer 2 at which amphibole disappears (Pl_{rim}: layer 1; Grt+Kfs±Amph: layer 2; Grt+Amp: layer 3; Cpx_{rim}: layer 4).

composed of symplectitic garnet+K-feldspar±amphibole. The amphibole in the inner layer is mostly present only in the portion of the corona close to the plagioclase. The outer rim (layer 3) consists of garnet+amphibole. The garnet coronas appear to have grown at the expense of both the plagioclase and the relict clinopyroxene, as shown by the different nature of the phases intergrown with garnet (Fig. 5) and the change in garnet composition (Fig. 6 — see Section 5.3 for discussion).

Orthopyroxene, olivine and titanite are present in few samples, and also show coronitic textures when in contact with plagioclase. Due to the minor amounts of these phases, we briefly describe the textures here, but do not attempt to model their coronas. Orthopyroxene is present in only one of the samples (434508). The orthopyroxene grains are also clouded by exsolution oxides, and have a recrystallized oxide-free rim of diopsidic clinopyroxene (10 to 20 μm thick). The clinopyroxene rim is surrounded by an irregular symplectitic garnet corona (30 to 50 μm thick), in which garnet is intergrown with K-feldspar and biotite. The garnet corona is bounded by a zoisite-free plagioclase rim (100 to 200 μm thick). Olivine is present in one sample (434507). The corona textures are similar to those described by Rivers and Mengel (1988). The olivine grains are surrounded by a 100–200 μm thick rim of orthopyroxene, which is in turn bounded by an irregular rim of amphibole. The outer corona is 100 to 200 μm thick and consists of symplectitic garnet plus amphibole. Titanite within plagioclase domains also develop coronas. The titanite grains are typically surrounded by an oxide corona, an orthopyroxene corona and a discontinuous amphibole corona. The outer corona is made of garnet.

4.2. Stage II

Stage II coronas are found in the outer part of the core of the leucogabbro body (e.g. 434501; Fig. 2). None of the Stage II samples have orthopyroxene, olivine or titanite. The igneous textures are still recognizable at the outcrop scale, although noticeable garnet coronas are present at the contact between plagioclase and clinopyroxene.

The zoisite within the plagioclase domains increases in size and abundance up to 40% modal volume (Fig. 4b). The zoisite-free plagioclase rim is still present, and equal in thickness to Stage I samples. The mottled appearance of the zoisite-free rim is more evident than in Stage I samples, and we interpret this as the result of continuing and more advanced consumption of zoisite. The recrystallized clinopyroxene rim thickens (to about 100 μm) (Fig. 3b), and at the core and along fractures of the relict clinopyroxene domains, the augitic grains are replaced by a very fine aggregate of microcrystalline amphibole, recrystallized clinopyroxene, plagioclase, quartz, titanite and carbonate. Locally, between the relict augite core and the newly formed clinopyroxene rim, a discontinuous, thin rim of amphibole is present (Fig. 4b). The garnet coronas are still discontinuous and irregular, but their thickness is greater than in Stage I (100 to 150 μm). The garnet coronas are no longer symplectitic. Amphibole and K-feldspar are no longer intergrown with garnet, but inclusions of plagioclase and zoisite (too small for accurate analyses to be performed) are now present in the garnet, especially in the outer part of the garnet coronas and in the bigger garnets nucleating in the Pl–Zo domains.

4.3. Stage III

Stage III samples are found in the intermediate zone of the leucogabbro body, and in particular in the felsic matrix surrounding the dark green clumps of eclogite (434515b; Figs. 2 and 3b).

Plagioclase domains in the core of the grains are clouded by numerous needles of zoisite (30 to 40% modal volume). Some small kyanite crystals (<5%) are also present at this stage, especially in the zoisite-free rim. Patchy scapolite is common within the plagioclase domains. Garnet crystals have nucleated and grown in the plagioclase, and also form coronas at the contacts between plagioclase and clinopyroxene (about 150 to 200 μm thick — Fig. 4c). The garnet has inclusions of plagioclase and quartz; these are too small to provide good analyses.

Clinopyroxene domains contain inclusions of amphibole and plagioclase, and are characterized by thin (10 to 50 μm), discontinuous rims of quartz and/or plagioclase (An_{22}). These rims are present whether the garnet corona is present or not.

4.4. Eclogite

Clumps of eclogite (sample 434515a; Figs. 2 and 3b) are surrounded by Stage III "matrix" (as described above) in the inner rim of the Bourbon body. The original location of plagioclase and pyroxene domains is still recognizable (Fig. 4d), because the plagioclase domain has been completely replaced by garnet, and the original pyroxene domain has been replaced by a patchy aggregate of omphacite (up to Jd_{33}), plagioclase, K-feldspar, and amphibole. Apatite is also locally present in the pyroxene domains.

4.5. Amphibolite

Strongly foliated amphibolite comprises the outer rim of the Bourbon Leucogabbro (sample 434523)

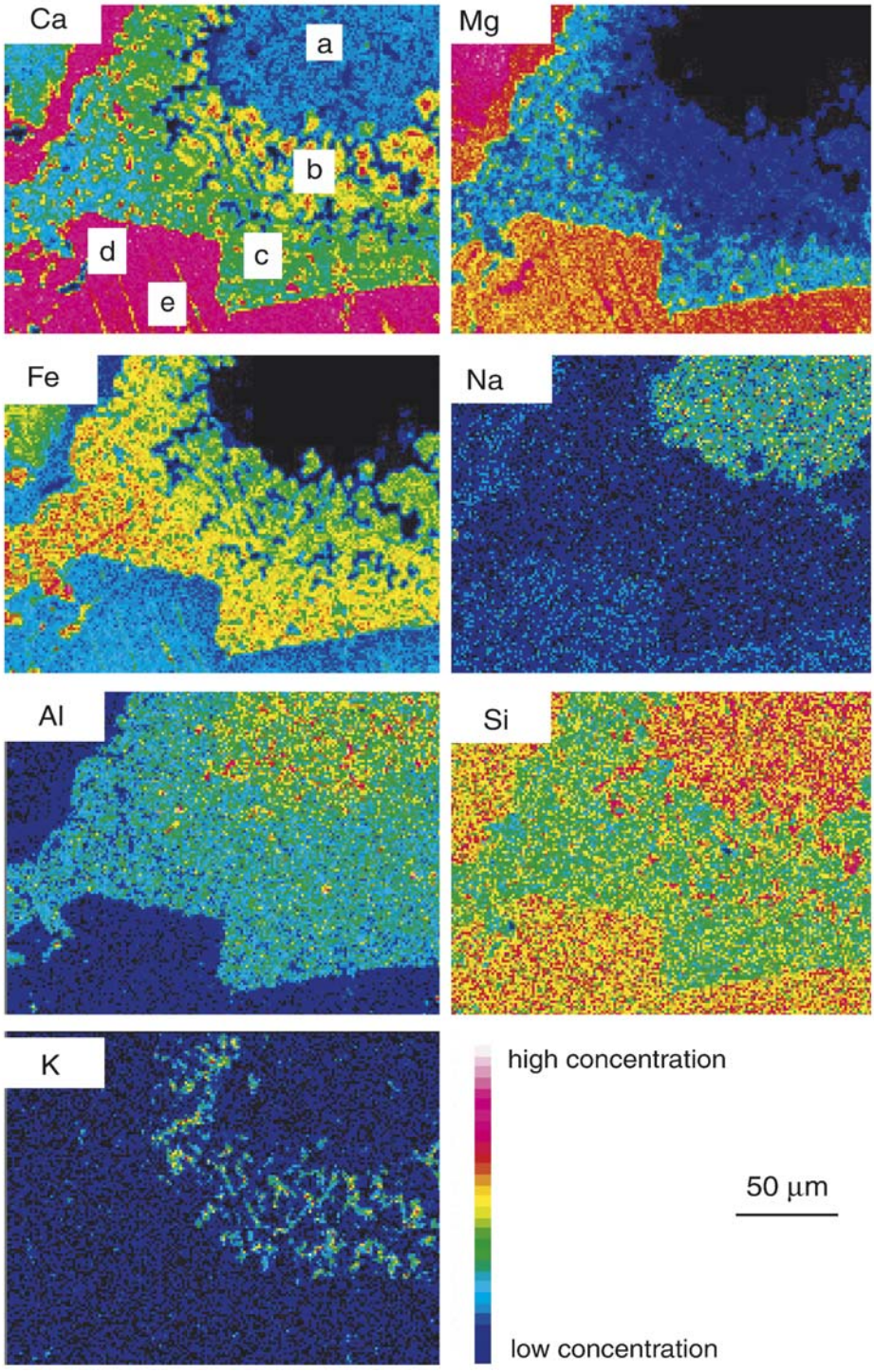

Fig. 6. Compositional maps showing the multi-layered corona representative of Stage I. (a) Plagioclase rim; (b) Garnet + K-feldspar ± Amphibole corona; (c) Garnet + Amphibole corona; (d) Clinopyroxene rim; (e) Relict clinopyroxene.

(Figs. 2 and 3c). These are the only retrogressed rocks in the entire lenticular metaleucogabbro body. Samples contain amphibole + plagioclase + quartz + zoisite + white mica + garnet + biotite (Table 2). Preferential orientation of subhedral to euhedral amphibole, zoisite, and white mica defines the strong foliation, implying their formation

Table 3
Chemistry of representative relict igneous pyroxenes in the core of the metaleucogabbro

Sample	Cpx	Opx
	434508	434508
SiO_2	49.961	52.151
TiO_2	1.005	0.027
Al_2O_3	1.749	0.328
FeO	15.754	29.682
MnO	0.184	0.392
MgO	11.877	18.447
CaO	16.698	0.332
Na_2O	1.808	0.016
K_2O	0.000	0.000
Cr_2O_3	na	0.000
NiO	0.957	0.000
Total	99.993	101.550
Mineral formulas (24 oxygens)		
Si	7.687	7.923
Ti	0.116	0.003
Al	0.317	0.058
Fe	2.027	3.771
Mn	0.024	0.050
Mg	2.724	4.178
Ca	2.753	0.054
Na	0.539	0.004
K	0.000	0.000
Cr	na	0.000
Ni	0.118	0.000

during amphibolite-facies retrogression. Garnet grains make up about 10% of the rock, and are subhedral to anhedral. The irregular, embayed boundaries of garnet suggest that the grains are relicts of the higher-pressure metamorphic assemblage that have been partially resorbed during retrogression.

5. Mineral chemistry

Representative chemical analyses of relict and metamorphic mineral phases for the different stages of eclogitization are given in Tables 3–7. All chemical analyses and X-ray maps were collected at the Department of Geology and Geophysics at the University of Minnesota, Minneapolis, Minnesota, using a JEOL 8900 electron microprobe operated with 5 WDS spectrometers at 15 kV and a current of 20 na.

The range of compositions in the different prograde and retrograde stages is reported for each mineral. Our nomenclature follows Morimoto et al. (1988) for the pyroxenes and Leake et al. (1997) for the amphiboles. Mineral abbreviations are after Spear (1993).

5.1. Plagioclase

The composition of the original igneous plagioclase is not preserved in the analyzed samples because the igneous plagioclase had already reacted to form zoisite, and in some cases kyanite. In the least reacted samples (Stage I), the most calcic composition is An_{40} (Table 4). This composition is found in the cores of the plagioclase grains, where zoisite is present. In the zoisite-free (<2%) rim, the composition is more sodic (An_{33}) (Table 4). We interpret the zoisite-free plagioclase rim as prograde, and due to zoisite consumption, rather than the result of igneous zoning. This is for two reasons: 1) There is no continuous zoning in the composition of the plagioclase going from the center to the margin of the plagioclase+zoisite portion of the plagioclase grains (An_{43} to An_{40} to An_{41}), and the plagioclase composition changes rather abruptly at the boundary between the plagioclase+zoisite core and the zoisite-free rim; and 2) the mottled appearance of the zoisite-free rim suggests replacement of zoisite. Our interpretation of the zoisite-free rim as a prograde metamorphic feature is supported by the fact that the composition of plagioclase becomes

Table 4
Chemistry of representative plagioclase from different metamorphic stages within the leucogabbro

Stage	I/ Zoisite	I/Rim	II	III	Eclogite	Amph
Sample	434508	434508	434501	434515b	434515a	434523
SiO_2	56.184	59.264	60.665	62.090	62.970	62.498
TiO_2	0.000	0.063	0.000	0.000	0.000	0.003
Al_2O_3	27.208	25.679	25.504	24.824	23.243	24.200
FeO	0.001	0.096	0.002	0.027	0.130	0.028
MnO	0.002	0.000	0.016	0.000	0.000	0.044
MgO	0.000	0.000	0.008	0.009	0.000	0.005
CaO	8.796	7.036	6.078	5.025	3.728	4.666
Na_2O	6.556	7.345	7.938	8.434	9.422	8.866
K_2O	0.245	0.272	0.283	0.284	0.204	0.077
Cr_2O_3	0.128	0.000	0.000	0.000	0.000	0.000
NiO	0.041	0.000	0.070	0.004	0.000	0.014
Total	99.161	99.755	100.564	100.703	99.697	100.401
Mineral formulas (24 oxygens)						
Si	7.635	7.948	8.048	8.193	8.377	8.263
Ti	0.000	0.006	0.000	0.000	0.000	0.0003
Al	4.358	4.059	3.988	3.861	3.644	3.771
Fe	0.0001	0.011	0.0003	0.003	0.014	0.003
Mn	0.0002	0.000	0.001	0.000	0.000	0.005
Mg	0.0001	0.000	0.001	0.001	0.000	0.0009
Ca	1.281	1.011	0.864	0.710	0.531	0.661
Na	1.727	1.910	2.042	2.158	2.430	2.273
K	0.042	0.046	0.047	0.047	0.034	0.012
Cr	0.013	0.000	0.000	0.000	0.000	0.000
Ni	0.004	0.000	0.007	0.0004	0.000	0.001

Table 5
Chemistry of representative clinopyroxene from different metamorphic stages within the leucogabbro

Sample	Relict	Stage I	Stage II	Stage III	Eclogite
	434508	434508	434501	434515b	434515a
SiO_2	49.961	52.246	53.451	53.411	53.449
TiO_2	1.005	0.097	0.088	0.218	0.207
Al_2O_3	1.749	2.152	4.406	9.003	8.930
FeO	15.754	11.416	4.475	4.011	4.293
MnO	0.184	0.124	0.069	0.002	0.020
MgO	11.877	11.569	13.477	11.010	10.932
CaO	16.698	20.149	19.779	18.173	17.647
Na_2O	1.808	1.950	2.957	3.671	3.733
K_2O	0.000	0.000	0.007	0.000	0.000
Cr_2O_3	na	0.000	na	0.000	0.000
NiO	0.957	0.025	0.005	0.000	0.003
Total	99.993	99.728	98.714	99.499	99.214
Mineral formulas (24 oxygens)					
Si	7.687	7.894	7.880	7.728	7.754
Ti	0.116	0.011	0.008	0.023	0.022
Al	0.317	0.383	0.764	1.535	1.527
Fe	2.027	1.442	0.552	0.485	0.521
Mn	0.024	0.015	0.008	0.0002	0.002
Mg	2.724	2.605	2.960	2.374	2.364
Ca	2.753	3.262	3.124	2.817	2.743
Na	0.539	0.571	0.844	1.029	1.050
K	0.000	0.000	0.001	0.000	0.000
Cr	na	0.000	na	0.000	0.000
Ni	0.118	0.003	0.0008	0.000	0.0003

progressively more sodic with increasing pressure (Goldsmith, 1982; Wayte et al., 1989). From Stage II to the Eclogite Stage, the An content of the plagioclase decreases from An_{30} to An_{20} (Table 4). The An content increases slightly during retrogression to amphibolite facies (An_{22}).

5.2. Pyroxene

Abundant relict igneous clinopyroxene and minor amounts of orthopyroxene are present. The composition of selected igneous and metamorphic pyroxenes is shown in Tables 3 and 5. The few orthopyroxenes are found in sample 434508 (Stage I), and fall within the En_{50}–En_{80} range. Relict clinopyroxenes are augitic to diopsidic in composition, while the recrystallized pyroxenes are diopside.

The recrystallized Stage I clinopyroxene rims are diopside (Jd_6) (Table 5). The Jd content of the metamorphic clinopyroxene increases progressively from Stage I (Jd_6) to Stage II (Jd_{13}) to the Eclogite Stage ($Jd_{26–33}$) (Table 5). Pyroxene is not preserved in the retrogressed amphibolites of the outer rim.

5.3. Garnet

Garnet coronas are commonly zoned (Fig. 6). The zoning is abrupt, and the change in composition seems to be related to the phase that garnet is replacing (Figs. 5 and 6). Garnet that texturally seems to have grown at the expenses of pyroxene has lower Ca, and greater Fe and Mg content. On the other hand, garnet that has grown at the expense of plagioclase has greater Ca, and lower Fe and Mg content.

Although the garnet composition is not constant in each stage, for the purpose of modeling we used an intermediate composition for each sample. The average composition of representative garnets for each stage is shown in Table 6. Garnet shows a steady change in both grossular and pyrope content with increasing transformation to eclogite. The grossular content decreases from Grs_{40} to Grs_{29} between Stage I to the Eclogite Stage. The pyrope content increases from Stage I to Stage II (Prp_{10} to Prp_{22}). The Prp content from Stages II to Eclogite Stage is essentially the same. Unlike the previous two end-members, almandine does not show a continuous trend. The almandine content decreases first from Stage I to Stage II (Alm_{51} to Alm_{41}), and then increases steadily from Stage II to Eclogite Stage (Alm_{41} to Alm_{49}). No significant change in X_{Grs}, X_{Prp} and X_{Alm} end-members

Table 6
Chemistry of representative garnets from different metamorphic stages within the leucogabbro

Sample	Stage I	Stage II	Stage III	Eclogite	Amphibolite
	434508	434501	434515b	434515a	434523
SiO_2	37.989	39.127	38.598	38.776	38.284
TiO_2	0.054	0.032	0.054	0.049	0.002
Al_2O_3	22.605	22.911	22.983	23.028	22.843
FeO	22.91	19.032	22.055	23.766	24.572
MnO	0.615	0.419	0.362	0.397	0.682
MgO	2.563	5.662	5.689	5.680	5.228
CaO	13.512	13.225	11.055	10.849	9.841
Na_2O	na	0.005	0.027	0.004	0.002
K_2O	na	0.004	0.005	0.002	0.000
Total	100.25	100.417	100.828	102.551	101.454
Mineral formulas (24 oxygens)					
Si	5.984	5.954	5.900	5.864	5.874
Ti	0.006	0.004	0.006	0.004	0.000
Al	4.152	4.11	4.140	4.106	4.130
Fe	2.986	2.422	2.818	3.006	3.152
Mn	0.082	0.054	0.046	0.052	0.088
Mg	0.596	1.284	1.296	1.280	1.196
Ca	2.256	2.156	1.810	1.758	1.616
Na	na	0.001	0.002	0.001	0.0008
K	na	0.0008	0.000	0.000	0.000

Table 7
Chemistry of representative amphiboles from different metamorphic stages within the leucogabbro

Sample	Stage I	Stage II	Eclogite	Amphibolite
	434508	434501	434515a	434523
	Si-edenite	Tremolite	Al-pargasitic	Hornblende
SiO_2	52.12	53.58	42.10	42.42
TiO_2	0.158	0.17	0.71	0.40
Al_2O_3	4.724	3.38	15.99	17.29
FeO	9.330	5.77	10.60	12.90
MnO	0.100	0.03	0.00	0.15
MgO	10.88	20.39	12.48	10.46
CaO	18.91	11.48	10.89	10.72
Na_2O	2.300	1.07	2.22	2.00
K_2O	0.037	0.31	1.78	0.73
Cr_2O_3	0.060	0.00	0.00	0.00
NiO	na	0.04	0.02	0.00
Total	98.62	98.97	99.23	99.70
Mineral formulas (24 oxygens)				
Si	7.841	7.818	6.419	6.422
Ti	0.016	0.019	0.081	0.046
Al	0.841	0.581	2.874	3.085
Fe	1.174	0.704	1.351	1.633
Mn	0.016	0.004	0.000	0.019
Mg	2.55	4.435	2.837	2.360
Ca	3.05	1.795	1.779	1.738
Na	0.67	0.303	0.656	0.586
K	0.008	0.058	0.346	1.141
Cr	0.003	0.000	0.000	0.000
Ni	na	0.002	0.003	0.000

occurs between the Eclogite and Amphibolite Stages. The spessartine end-member is present in minor amounts and does not vary significantly.

5.4. Amphibole

Amphibole compositions are shown in Table 7. Stage I amphibole is found as part of the symplectitic coronas intergrown with garnet and has the composition of a silicic-edenite. Stage II amphiboles are found in two settings: as a discontinuous rim between the relict clinopyroxene and the recrystallized clinopyroxene rim, and as a minor part of microcrystalline aggregates together with recrystallized clinopyroxene, plagioclase, quartz, titanite and carbonate. Amphiboles in Stage II samples are tremolitic. Stage III samples contain no amphiboles, while eclogites contain aluminum rich pargasitic hornblende as microcrystalline aggregates intergrown with omphacite, K-feldspar and plagioclase. Unexpectedly, amphibole from the retrogressed foliated amphibolites is also pargasitic hornblende.

6. Reaction modeling

6.1. The model

Two assumptions were made in order to model the Stage I coronitic textures: 1) the coronitic textures are prograde features representing different "frozen" stages of the transformation of the leucogabbro-norite to eclogite; and 2) the system was open at the time of metamorphism.

Corona textures, especially symplectitic ones, are often considered cooling and retrograde features. In this study, we treat the coronas in the Bourbon metaleucogabbro-norite as prograde features. This assumption is supported by the mineral phases present in the system. The relict plagioclase in the coronitic stages is clouded by zoisite needles, which become progressively more abundant and larger from Stage I to Stage III. Stage III samples also contain small kyanite needles within the plagioclase. Furthermore, the Jd content of the recrystallized clinopyroxene progressively increases from Stage II to the Eclogite Stage, going from diopside to omphacite. These observations can be explained by the following reactions: increasing pressure in presence of water will break down calcic plagioclase according to the reaction

$$Pl + H_2O \rightarrow Zo + Ky + Qtz + Na\text{–}Pl$$

(Goldsmith, 1982). A further increment in pressure, in a system in which water is still available, will further break down plagioclase to give jadeite.

$$Pl + H_2O \rightarrow Jd + Zo + Ky + Qtz + Na\text{–}Pl$$

(Wayte et al., 1989). The garnet in the coronas can be explained by a modified version of the continuous reaction by Wayte et al. (1989)

$$Pl + Cpx \rightarrow Grt + Ky + Qtz + Na\text{–}Pl$$

by taking the continuous reaction for the pure Ca system and adding the components from the breakdown of clinopyroxene.

Amphibole in the corona layers is also believed to be prograde. Amphiboles in all the coronitic samples are edenitic and pargasitic, with relatively high Na+K values, consistent with higher metamorphic grade. Furthermore, pervasive retrograde amphibolitization is not observed in any of the samples from the core or the inner rim of the metaleucogabbro-norite.

Prograde symplectitic coronas in similar rocks have been amply described by Mørk (1985a,b, 1986), Pognante (1985), Gilotti and Elvevold (1998), and Lang and Gilotti (2001). The only other corona texture between plagioclase and clinopyroxene modeled in the literature was

described by Ashworth et al. (1992). Their coronas were retrograde features, with no garnet in the layers or zoisite from the breakdown of plagioclase.

The open-system assumption is supported by a plot of the composition of the reactants versus products of the Stage I coronas (Fig. 7). The exceptions are Si and Al (Fig. 7), which are conserved throughout the system. Furthermore, extensive trials to model the Bourbon coronas with an isochemical model resulted in poor outcome.

Corona-forming reactions in the literature have been modeled since the early seventies (Griffin and Heier, 1973; Whitney and McLelland, 1973). Early studies used mass-balance and steady-state diffusion equations to model corona sequences in a closed system, following Joesten (1977). More recent studies agree that spatially well-organized coronas cannot be completely explained by steady-state diffusion in isochemical systems. Joesten's (1977) method has been modified by Ashworth and Birdi (1990) and Johnson and Carlson (1990) to allow for an open-system behavior. These open-system grain boundary diffusion models (OSGBD) give the relative amount of mineral phases in the distinct corona layers once the layer sequence and the mineral phases in each layer are specified.

The OSGBD approach has been successfully used to model retrograde coronas between plagioclase and olivine (Ashworth and Birdi, 1990; Johnson and Carlson, 1990; Ashworth and Sheplev, 1997), plagioclase and orthopyroxene (Attoh, 1998), and plagioclase and clinopyroxene (Ashworth et al., 1992). We have used the open-system approach of Ashworth and Birdi (1990) and Ashworth and Sheplev (1997) to model the prograde Stage I coronas between relict plagioclase and relict clinopyroxene.

The Stage I corona sequence modeled in this paper is shown in Figs. 5 and 6. The four corona layers between the relict plagioclase and clinopyroxene are: a zoisite-free plagioclase rim adjacent to plagioclase (Pl_{rim} — layer 1), a symplectitic garnet plus K-feldspar plus or minus amphibole layer (layer 2), a symplectitic garnet plus amphibole layer (layer 3), and a recrystallized clinopyroxene rim (Cpx_{rim} — layer 4) adjacent to the augitic igneous clinopyroxene (Cpx_{rel}). Although layer 2 only shows amphibole in the portion closer to layer 1, and should actually be portrayed as two separate layers, we modeled this as one single layer for simplicity.

The main assumptions made in the model are: 1) Transport occurs by pure diffusion. Advection through coronas is unlikely (Ashworth and Sheplev, 1997). Even if the corona development is initially driven by interface kinetics, the diffusion process becomes the dominant mechanism as soon as the corona starts to form and the diffusion distances increase (Fisher, 1978). 2) Diffusion is one-dimensional and perpendicular to the boundaries between corona layers. 3) The fluxes of components within layers are constant. 4) Although the rock is in overall disequilibrium, there is local equilibrium between contiguous mineral phases and intergranular fluids. Local equilibrium is supported by the absence of complicated structures such as repetitive banding (Ashworth and Sheplev, 1997; Balashov and Lebedeva, 1991; Zharikov and Zaraisky, 1991). 5) The mineral compositions are fixed, and do not change over time. 6) The concentration of components in the diffusive medium at the boundaries between corona layers is constant over time, due to the fact that a local quasi-stationary state is reached (Fisher, 1973; Fisher and Lasaga, 1981). 7) The overall reaction remains constant.

The first inputs necessary to our model are the stoichiometric coefficients from the overall reaction. To uniquely define the overall reaction we used the approach described by Joesten and Fisher (1988), Ashworth and Birdi (1990), and Johnson and Carlson (1990). This method does not limit the number of components modeled for, and uses the measured proportion of mineral phases in the corona layers to determine an open-system reaction in which the boundary fluxes represent the metasomatic interaction with the surrounding rock. The data used to model Stage I coronas (Fig. 5) are the mineral compositions (Table 8), the observed modal proportions of the mineral phases forming the corona layers measured in the corona as a whole (Pl_{rim}, Grt, Kfs, Amp, and Cpx_{rim}), and the selected values of the diffusion coefficient ratios, L (Table 9).

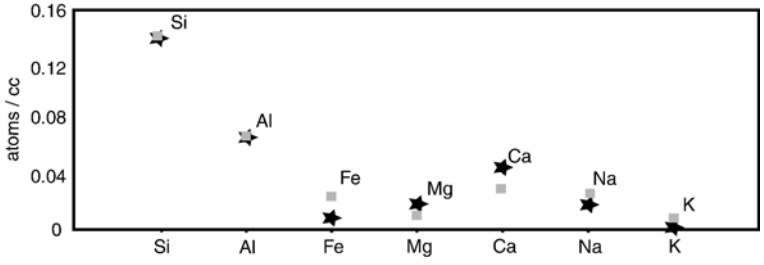

Fig. 7. Plot of the amount of each element in the reactants (Pl_Zo and Cpx_{rel} — black stars) versus the amount in the products forming the corona layers (Pl_{rim}, Grt, Kfs, Amp, Cpx_{rim} — gray squares). The diagram shows how Si and Al are conserved in this system.

Table 8
Representative phase compositions used in the open-system modeling of Stage I coronas

	i=Si	i=Al	i=Fe	i=Mg	i=Ca	i=Na	i=K
k=Pl_Zo	7.036	4.691	0	0.009	2.052	1.173	0.020
k=Pl_{rim}	7.948	4.050	0.011	0	0.951	2.024	0.051
k=Grt	5.920	4.152	2.986	1.052	2.026	0	0
k=Kfs	8,902	3.143	0.010	0	0.003	0.377	2.554
k=Amp	7.841	0.840	1.174	2.550	3.050	0.670	0.008
k=Cpx_{rim}	7.894	0.383	1.443	2.606	3.262	0.571	0
k=Cpx_{rel}	7.851	0.437	1.293	3.155	2.941	0.440	0.0004

The observed modal amounts of the different phases forming the coronas are estimated at: Pl_{rim} 52%, Grt 27%, Kfs 7%, Amp 5%, and Cpx_{rim} 9%. The modal amounts were estimated comparing multiple coronas in Stage I samples, and averaging them. The molar ratios used in the model are calculated by dividing the modal amounts by the molar volume, and then by normalizing to Cpx_{rim}=1. The resulting molar ratios are:

$$Pl_{rim} : Grt : Kfs : Amp : Cpx_{rim} = 5.06 : 3.18 : 0.62 : 0.53 : 1 \quad (1)$$

We can then calculate the overall reaction by writing a mass-balance equation for each component i which is constrained (Ashworth and Birdi, 1990) by:

$$\sum_{k=1}^{\Phi} \upsilon_k n_{ik} = 0 \quad (2)$$

where n_{ik} is the amount of component i in phase k (Table 8), υ_k is the stoichiometric coefficient from the overall reaction for each phase k, and Φ is the number of phases in the system. We fixed Al and Si assuming that the system is closed with respect to these two components. Al and Si are commonly considered to be conserved in this type of system (Mongkoltip and Ashworth, 1983; Ashworth and Birdi, 1990), and closure to Si and Al is confirmed in our case by a comparison between the amount of the two components in the reactants versus their amount in the multi-layer corona as a whole (Grant, 1986). Fig. 7 shows that Si and Al are the only two components conserved in the system. In some previous models, volume was held constant together with one component to define the overall reaction (Johnson and Carlson, 1990). We prefer the former approach because it allows for eventual volume losses common during high-pressure metamorphism. Furthermore, we tried constraining volume and Si, and volume and Al, with little change in the final product.

Using these assumptions, the two conservation equations are then:

$$7.036\ \upsilon_{Pl-Zo} + 7.948\ \upsilon_{Plrim} + 5.92\ \upsilon_{Grt} + 8.902\ \upsilon_{Kfs} + 7.841\ \upsilon_{Amp} + 7.894\ \upsilon_{Cpxrim} + 7.850\ \upsilon_{Cpxrel} = 0 \quad (3)$$

$$4.691\ \upsilon_{Pl-Zo} + 4.050\ \upsilon_{Plrim} + 4.152\ \upsilon_{Grt} + 3.143\ \upsilon_{Kfs} + 0.84\ \upsilon_{Amp} + 0.383\ \upsilon_{Cpxrim} + 0.436\ \upsilon_{Cpxrel} = 0 \quad (4)$$

where Eqs. (3) and (4) represent closure of the system with respect to Si and Al respectively (Pl–Zo is plagioclase with zoisite inclusions, Cpx_{rel} is the relict igneous clinopyroxene core, Pl_{rim} is the zoisite-free rim, Grt is garnet, Kfs is K-feldspar, Amp is amphibole, and Cpx_{rim} is the recrystallized clinopyroxene rim).

These equations can be solved by specifying that 1 mol of Pl–Zo is consumed per mole of reaction progress (υ_{Pl-Zo}=1), and by using the calculated molar ratios: υ_{Plrim}=5.06 υ_{Cpxrim}, υ_{Grt}=3.18 υ_{Cpxrim}, υ_{Kfs}=0.62 υ_{Cpxrim}, υ_{Amp}=0.53 υ_{Cpxrim}. These factors are replaced in Eqs. (3) and (4), and the simultaneous solution of the two equations gives the stoichiometric coefficients of the overall reaction.

Since the system is open, we also need to account for metasomatic fluxes. These are treated as an imaginary phase (Met_Flux), where υ_{Met_Flux} is set to 1. Unlike the model of Ashworth and Sheplev (1997) in which two metasomatic phases were allowed into the system at the two boundaries between the reactants and their contiguous corona layers, in our model the metasomatic phase enters the system at boundary 3 (Figs. 5 and 8). The choice of boundary 3 was dictated by microstructural evidence. Fig. 5 shows a significant change in the nature of the phases intergrown with garnet, which suggests that the original boundary between relict plagioclase and relict clinopyroxene was located at this site.

Table 9
Diffusion coefficients ratios (L-ratios) used in the modeling of Stage I coronas

	L_{SiSi}/L_{ii}
i=Si	1
i=Al	0.9
i=Fe	2.8
i=Mg	0.1
i=Ca	1
i=Na	3
i=K	1.2
$L_{MgMg} > L_{AlAl} > L_{SiSi} > L_{CaCa} > L_{KK} > L_{FeFe} > L_{NaNa}$	

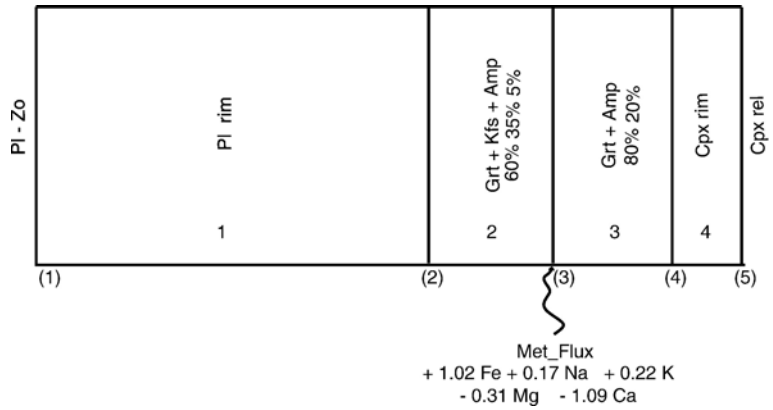

Fig. 8. Sketch of the Stage I corona sequence as resulted from the open-system steady-state grain boundary diffusion model (Ashworth and Birdi, 1990; Ashworth and Sheplev, 1997).

The metasomatic fluxes for each component i are calculated using the equation

$$-\sum \mathrm{n}_{ik}\upsilon_k \tag{5}$$

where n_{ik} is the amount of component i in phase k and υ_k is the stoichiometric coefficient from the overall reaction for each phase k. We use the sign convention of Ashworth and Sheplev (1997), such that moles of product phases are negative. This sign convention has the advantage that fluxes coming into the system will have a positive sign, while the fluxes leaving the system will have a negative sign.

The overall reaction calculated for Stage I using Eqs. (3)–(5) is the following:

$$\begin{aligned}1\ \mathrm{Pl}-\mathrm{Zo} + 0.406\ \mathrm{Cpx_{rel}} + 1.026\ \mathrm{Fe}\\ + 0.170\ \mathrm{Na} + 0.226\ \mathrm{K} \rightarrow 0.675\ \mathrm{Pl_{rim}}\\ + 0.424\ \mathrm{Grt} + 0.083\ \mathrm{Kfs} + 0.071\ \mathrm{Amp}\\ + 0.133\ \mathrm{Cpx_{rim}} + 0.316\ \mathrm{Mg} + 1.093\ \mathrm{Ca}\end{aligned} \tag{6}$$

Once the overall reaction is defined, the local boundary reactions are determined by varying the postulated values of the L-ratios (diffusion coefficient ratios), which change the distribution of the different mineral phases among the four layers. After extensive trial and error with different L-values (Table 9)), the modeled corona (Fig. 8) closely matches the observed one. The reaction coefficients υ were estimated at each boundary in sequence, from left to right (Fig. 8). The key equation for each boundary q between two contiguous corona layers is (Ashworth and Sheplev, 1997):

$$\sum_{k=1}^{\Phi^q} A_{mk} \sum_{r=1}^{q} \upsilon_k^r = -\sum_{k=\Phi^q+1}^{\Phi^q+\Phi^{\mathrm{left}}} A_{mk}(\upsilon'_k)^q \tag{7}$$

Eq. (7) gives the stoichiometric coefficients of phase k produced or consumed at boundary q (υ_k^q). The left portion of the equation represents phases present in layer q (Φ^q), while the right portion of the equation represents phases present to the left of boundary q but not in layer q (Φ^{left}).

A is a coefficient defined by the equation

$$A_{km} = \sum_{i=1}^{S} (L_{\mathrm{SiSi}}/L_{ii}) n_{ik} n_{im} \tag{8}$$

Eq. (8) is calculated for each possible pair of mineral phases k and m in the system (S is the number of components in the model, L_{SiSi}/L_{ii} is the ratio of the diffusion coefficients for the individual components i related to the

Table 10
Calculated A_{mk} coefficients

	m=Plag_Zo	m=Plag$_{\mathrm{rim}}$	m=Grt	m=Ksp	m=Amp	m=Cpx$_{\mathrm{rim}}$
k=Pl_Zo		82.096	63.341	77.298	67.335	65.865
k=Pl$_{\mathrm{rim}}$	82.096	91.130	64.205	84.658	72.387	70.751
k=Grt	63.341	64.205	79.742	64.534	65.821	67.111
k=Kfs	77.298	84.658	64.534	96.390	73.001	72.052
k=Amp	67.335	72.387	65.821	73.001	77.275	78.691
k=Cpx$_{\mathrm{rim}}$	65.865	70.751	67.111	72.052	78.691	80.575
k=Met_Flux		0.0382	6.3299	0.9110	0.3016	0.7882

diffusion coefficient of Si, and n_{ik} is the amount of component i in phase k).

The values calculated for all the A_{mk} quantities for this system are shown in Table 10. To model the layer sequence observed in Stage I (Fig. 8), the quantities A_{mk} are used in Eq. (7) for each boundary q in turn, starting with boundary 1. There will be the same number of equations at each boundary as the number of mineral phases that are present to the right of the boundary itself. This process calculates the reaction coefficients $\upsilon^q{}_k$ at each boundary.

At boundary (1), Pl_Zo/Pl_{rim}, Eq. (7) is

$$A_{\mathrm{PlPlag}}\ \upsilon^1_{\mathrm{Pl}} = -A_{\mathrm{PlPl\_Zo}}\upsilon_{\mathrm{Pl\_Zo}} \tag{9}$$

where $\upsilon_{\mathrm{Pl\_Zo}}$ is the stoichiometric coefficient from the overall reaction.

At boundary 2, Pl_{rim}/Grt+Kfs+Amp, there are three equations to be solved, one for each of the three phases in layer 2 (Fig. 8)

$$\begin{aligned} &A_{\mathrm{GrtGrt}}\upsilon^2_{\mathrm{Grt}} + A_{\mathrm{GrtKfs}}\upsilon^2_{\mathrm{Kfs}} + A_{\mathrm{GrtAmp}}\upsilon^2_{\mathrm{Amp}} \\ &\quad = -A_{\mathrm{GrtPl}}\upsilon_{\mathrm{Pl}} - A_{\mathrm{GrtPl\_Zo}}\upsilon_{\mathrm{Pl\_Zo}} \end{aligned} \tag{10}$$

$$\begin{aligned} &A_{\mathrm{GrtKfs}}\upsilon^2_{\mathrm{Grt}} + A_{\mathrm{KfsKfs}}\upsilon^2_{\mathrm{Kfs}} + A_{\mathrm{KfsAmp}}\upsilon^2_{\mathrm{Amp}} \\ &\quad = -A_{\mathrm{KfsPl}}\upsilon_{\mathrm{Pl}} - A_{\mathrm{KfsPl\_Zo}}\upsilon_{\mathrm{Pl\_Zo}} \end{aligned} \tag{11}$$

$$\begin{aligned} &A_{\mathrm{GrtAmp}}\upsilon^2_{\mathrm{Grt}} + A_{\mathrm{AmpKfs}}\upsilon^2_{\mathrm{Ksp}} + A_{\mathrm{AmpAmp}}\upsilon^2_{\mathrm{Amp}} \\ &\quad = -A_{\mathrm{AmpPl}}\upsilon_{\mathrm{Pl}} - A_{\mathrm{AmpPl\_Zo}}\upsilon_{\mathrm{Pl\_Zo}} \end{aligned} \tag{12}$$

where υ_{Pl} is the stoichiometric coefficient from the overall reaction and

$$\upsilon^2_{\mathrm{Pl}} = \upsilon_{\mathrm{Pl}} - \upsilon^1_{\mathrm{Pl}} \tag{13}$$

At boundary 3, Grt+Kfs±Amp/Grt+Amp, there will be two equations, since there are two phases to the right of the boundary. At this boundary we also allow the metasomatic flux to come into the system (Met_Flux). The equations for this boundary are then

$$\begin{aligned} &A_{\mathrm{GrtGrt}}\upsilon_{\mathrm{Grt}} + A_{\mathrm{GrtAmp}}\upsilon_{\mathrm{Amp}} \\ &\quad = -A_{\mathrm{GrtPl}}\upsilon_{\mathrm{Pl}} - A_{\mathrm{GrtPl\_Zo}}\upsilon_{\mathrm{Pl\_Zo}} \\ &\qquad -A_{\mathrm{GrtKfs}}\upsilon_{\mathrm{Kfs}} - A_{\mathrm{GrtMet\_Flux}}\ \upsilon_{\mathrm{Met\_Flux}} \end{aligned} \tag{14}(a)$$

$$\begin{aligned} &A_{\mathrm{GrtAmp}}\upsilon_{\mathrm{Grt}} + A_{\mathrm{AmpAmp}}\upsilon_{\mathrm{Grt}} \\ &\quad = -A_{\mathrm{AmpPl}}\upsilon_{\mathrm{Pl}} - A_{\mathrm{AmpPl\_Zo}}\upsilon_{\mathrm{Pl\_Zo}} \\ &\qquad -A_{\mathrm{AmpKfs}}\upsilon_{\mathrm{Kfs}} - A_{\mathrm{AmpMet\_Flux}}\ \upsilon_{\mathrm{Met\_Flux}} \end{aligned} \tag{15}(b)$$

where υ_{Grt}, υ_{Kfs}, $\upsilon_{\mathrm{Met\_Flux}}$, and υ_{Amp} are the stoichiometric coefficients from the overall reaction, and

$$\upsilon^3_{\mathrm{Grt}} = \upsilon_{\mathrm{Grt}} - \upsilon^2_{\mathrm{Grt}} \tag{16}$$

$$\upsilon^3_{\mathrm{Amp}} = \upsilon_{\mathrm{Amp}} - \upsilon^2_{\mathrm{Amp}} \tag{17}$$

$$\upsilon^3_{\mathrm{Kfs}} = \upsilon_{\mathrm{Kfs}} - \upsilon^2_{\mathrm{Kfs}} \tag{18}$$

At boundary 4, Grt+Amp/Cpx_{rim}, there is only one Eq. (7)

$$\begin{aligned} &A_{\mathrm{CpxrimCpxrim}}\upsilon^4_{\mathrm{Cpxrim}} = -A_{\mathrm{CpxrimPl}}\upsilon_{\mathrm{Pl}} \\ &\quad -A_{\mathrm{CpxrimPl\_Zo}}\upsilon_{\mathrm{Pl\_Zo}} - A_{\mathrm{CpxrimKfs}}\upsilon_{\mathrm{Kfs}} \\ &\quad -A_{\mathrm{CpxrimGrt}}\upsilon_{\mathrm{Grt}} - A_{\mathrm{CpxrimAmp}}\upsilon_{\mathrm{Amp}} \\ &\quad -A_{\mathrm{CpxrimMet\_Flux}}\upsilon_{\mathrm{Met\_Flux}} \end{aligned} \tag{19}$$

where

$$\upsilon^4_{\mathrm{Grt}} = \upsilon_{\mathrm{Grt}} - (\upsilon^2_{\mathrm{Grt}} + \upsilon^3_{\mathrm{Grt}}) \tag{20}$$

$$\upsilon^4_{\mathrm{Amp}} = \upsilon_{\mathrm{Amp}} - (\upsilon^2_{\mathrm{Amp}} + \upsilon^3_{\mathrm{Amp}}) \tag{21}$$

Finally at the fifth boundary, Cpx_{rim}/Cpx_{rel}, the amount of clinopyroxene produced is

$$\upsilon^5_{\mathrm{Cpxrim}} = \upsilon_{\mathrm{Cpxrim}} - \upsilon^4_{\mathrm{Cpxrim}} \tag{22}$$

where $\upsilon_{\mathrm{Cpxrim}}$ is the stoichiometric coefficient from the overall reaction.

Table 11
Stoichiometric coefficients at boundaries 1 through 5 calculated with our open-system model

	$\upsilon_{\mathrm{Plrim}}$	υ_{Grt}	υ_{Kfs}	υ_{Amp}	$\upsilon_{\mathrm{Cpxrim}}$
Bound 1	−0.090	0	0	0	0
Bound 2	0.226	−0.172	−0.084	−0.013	0
Bound 3	0	−0.256	0.0008	0.214	0
Bound 4	0	0.004	0	−0.271	0.262
Bound 5	0	0	0	0	−0.395

Stoichiometric coefficients (in moles) at boundaries 1 through 5 as resulting from model (Eqs. (9)–(22)). Negative sign indicates phases produced at a boundary and positive sign indicates phases consumed, following the convention of Ashworth and Sheplev (1997).

The molar amount of plagioclase in layer 1 is the difference between the amount produced at boundary 1 and the amount consumed at boundary 2, just as the number of moles of K-feldspar in layer 2 is given by the difference between the amount produced at boundary 2 and the amount consumed at boundary 3. When it comes to the number of moles of garnet and amphibole in layers 2 and 3 however, the molar amounts are affected by the transfer rate of garnet through boundary 3. We need then to determine the amounts transferred to layer 3

$$\upsilon^3_{\mathrm{Kfs}} * (\upsilon^2_{\mathrm{Grt}} \,/\, \upsilon^2_{\mathrm{Kfs}}) = x \tag{23}$$

$$\upsilon^3_{\mathrm{Kfs}} * (\upsilon^2_{\mathrm{Amp}} \,/\, \upsilon^2_{\mathrm{Kfs}}) = y \tag{24}$$

so that the number of moles of garnet and amphibole in layer 2 is

$$-\upsilon^2_{\mathrm{Grt}} - x \tag{25}$$

$$-\upsilon^2_{\mathrm{Amp}} - y \tag{26}$$

and in layer 3

$$-\upsilon^3_{\mathrm{Grt}} - \upsilon^4_{Grt} + x \tag{27}$$

$$-\upsilon^3_{\mathrm{Amp}} - \upsilon^4_{\mathrm{Amp}} + y \tag{28}$$

6.2. Results of the model

The stoichiometric coefficients at each boundary calculated with Eqs. (9)–(11) are shown in Table 11. The molar amounts of mineral in the different layers are shown in Table 12. If we multiply the molar amounts in each layer by their corresponding molar volumes (Table 13), we obtain the volume in cubic centimeters of each corona layer and hence their thickness. Fig. 8 shows the result of our model.

According to our model (Table 11), the zoisite-free plagioclase rim is all produced at boundary 1 (Fig. 8). Part of the plagioclase rim is then consumed at boundary 2, where garnet, K-feldspar, and amphibole are produced. Boundary 3 is marked by the consumption of K-feldspar and amphibole. Amphibole is apparently consumed at this boundary in greater amounts than were produced at boundary 2. This is consistent with textural evidence (Fig. 5) that shows amphibole intergrown with garnet in layer 2 mostly in the layer portion closer to boundary 2. Boundary 3 is also characterized by production of garnet. Boundary 4 shows both clinopyroxene rim (from layer 4) and garnet (from layer 3) being consumed, while amphibole is produced. Finally, at boundary 5 the clinopyroxene rim is produced at the expense of the relict clinopyroxene. Comparing the ratios of modeled layer thickness for Pl_{rim}:Grt+Ksp+Amp:Grt+Amp:Cpx_{rim} to the observed one (as averaged from multiple Stage I coronas), we conclude that this approach satisfactorily modeled our system. In fact, the observed ratio of 3:1.3:0.95:0.5 is very close to the modeled one of 2.7:1.1:1:0.5.

Table 12
Molar amounts of different phases in individual layers that resulted from open-system modeling of Stage I coronas

	Pl_{rim}	Grt	Kfs	Amp	Cpx_{rim}
Layer 1	0.675	0	0	0	0
Layer 2	0	0.170	0.083	0.013	0
Layer 3	0	0.254	0	0.058	0
Layer 4	0	0	0	0	0.133

Table 13
Values of molar volumes used in the model

Pl	302.10
Grt	250.60
Kfs	326.16
Amp	272.92
Cpx	264.36

The values are in cc/mol and are calculated for 24 oxygens.

7. Discussion

After numerous attempts to produce the Bourbon coronas with isochemical models, we concur with most recent studies that spatially well-organized coronas are not fully explained by steady-state diffusion in isochemical systems. We modeled Stage I corona sequences with OSGBD theories following Ashworth and Sheplev (1997). The results of our model match quite closely the observed textures, not only in the thickness and mineral distribution within the individual layers (Fig. 8), but also in the smaller scale textural variations within the individual layers. The ratios between the average thicknesses of the corona layers observed in Stage I samples are Pl_{rim}:Grt+Kfs+Amp:Grt+Amp:Cpx_{rim} equal to 3:1.3:0.95:0.5. These ratios are very close to the modeled ones of 2.7:1.1:1:0.5. Furthermore, Fig. 5 shows Stage I coronas, and in particular how amphibole within layer 2 is only present in the portion of layer 2 closer to boundary 2. This can be explained by our model, because amphibole is consumed at boundary 3 in greater amount that it is produced at boundary 2.

Our model shows that the observed corona sequence is only stable if we allow a gain in Fe, K, and Na, and a loss in Ca and Mg, with relative mobilities of the different components within the corona layers being $L_{MgMg} > L_{AlAl} > L_{SiSi} > L_{CaCa} > L_{KK} > L_{FeFe} > L_{NaNa}$. The fact that the system is open and contains mineral phases such as scapolite and zoisite implies that fluid circulation was active to some degree during the transformation to eclogite. Different degrees of eclogitization between the core and the inner rim, and within the inner rim itself (dark clumps versus lighter matrix) can then be explained by variations in fluid availability. Fluids would have acted as catalysts promoting further reactions to give more advanced eclogitization in some areas (Fig. 3a and b). Dehydration of igneous biotite (Table 2) could have provided initial fluids to promote eclogitization (Lang and Gilotti, 2001), thus leading to the formation of coronitic textures in the core of the leucogabbro. Fluids coming into the system from the surrounding orthogneisses, but not reaching the core of the body, could explain the greater degree of eclogitization and deformation of the inner rim, and the presence of eclogite clumps. The presence of symplectitic coronas only at the very center of the metaleucogabbro supports different fluid availability between the core and the inner rim. Ashworth and Chambers (2000) determined that formation of symplectites is inhibited by the presence of fluids.

Another possible explanation for the fist size clumps of eclogite surrounded by the coronitic matrix in the inner rim is that the protolith was greatly heterogeneous, and the completely eclogitized clumps represent more mafic areas within the leucogabbro (see San Gabriel anorthosite, Carter, 1987). A problem with this explanation, is that it is hard to envision such drastic heterogeneities at such a small scale. The leucogabbro body is 50 m wide by 200 m long. Heterogeneities are not observed in the core of the body, and the transition between the coronitic core and the inner rim with the completely eclogitized clumps is very sharp (over an area of 20 to 50 cm).

The results of our model, and the outcrop scale textural variations in the Bourbon metaleucogabbro-norite, allow us to evaluate the role played by open-system diffusion in the development of coronas. Although the strong spatial organization of the corona layers implies diffusion controlled reactions (Fisher, 1977), our model demonstrates the importance of external fluxes in the form of fluids coming into the system. External fluxes, in addition to element mobility, play a very important role in determining mineral stability, volume proportions, and mineral distribution within individual corona layers.

8. Conclusions

The data presented in this paper lead to the following conclusions:

1) The coronitic textures in the Bourbon Leucogabbro are prograde features, and record different stages of the transformation between leucogabbro-norite and eclogite.
2) The metamorphic system in which these textures formed was open. The corona sequence is stable if we allow a gain in Fe, K, and Na, and a loss in Ca and Mg, with relative mobilities of the different components within the corona layers $L_{MgMg} > L_{AlAl} > L_{SiSi} > L_{CaCa} > L_{KK} > L_{FeFe} > L_{NaNa}$.
3) Fluids played an important role in the eclogitization process. Different degrees of fluid availability and perhaps heterogeneities within the leucogabbro-norite are the cause for the different degrees of eclogitization in the different zones of the Bourbon metaleucogabbro-norite.
4) Open-system grain boundary diffusion theories give good results in modeling prograde textures in high pressure tectonic settings, with modeled coronas matching the observed coronas satisfactorily.

Acknowledgements

Mapping and sample collection for this project were completed by J. Gilotti and S. Elvevold in 1995 with funding from the Geological Survey of Denmark and Greenland (GEUS) and National Science Foundation grant EAR-9508218 to J.A.G. The National Geographic Society grant 6853-00 and NSF EAR-0208236 (to J.A.G.) also supported this project. Sartini-Rideout's travel funds to present this work at the 32nd IGC were provided by the Geoscience Department, the Graduate Senate, and the Graduate College at the University of Iowa.

References

Ashworth, J.R., Birdi, J.J., 1990. Diffusion modeling of coronas around olivine in an open system. Geochimica et Cosmochimica Acta 54, 2389–2401.

Ashworth, J.R., Sheplev, V.S., 1997. Diffusion modeling of metamorphic layered coronas with stability criterion and consideration of affinity. Geochimica et Cosmochimica Acta 61, 3671–3689.

Ashworth, J.R., Chambers, A.D., 2000. Symplectitic reaction in olivine and the controls of intergrowth spacing in symplectites. Journal of Petrology 41 (2), 285–304.

Ashworth, J.R., Birdi, J.J., Emmett, T.F., 1992. Diffusion in coronas around clinopyroxene: modeling with local equilibrium and steady state, and a non-steady-state modification to account for zoned actinolite-hornblende. Contributions to Mineralogy and Petrology 109, 307–325.

Attoh, K., 1998. Models for orthopyroxene-plagioclase and other corona reactions in metanorites, Dahomeyde orogen, West Africa. Journal of Metamorphic Geology 16, 345–362.

Balashov, V.N., Lebedeva, M.I., 1991. Macrokinetic model of origin and development of a monomineralic bimetasomatic zone. In: Perchuk, L.L. (Ed.), Progrss in Metamorphic and Magmatic Petrology. Cambridge University Press, pp. 167–195.

Brueckner, H.K., Gilotti, J.A., Nutman, A.P., 1998. Caledonian eclogite-facies metamorphism of Early Proterozoic protoliths from the North-East Greenland Eclogite Province. Contributions to Mineralogy and Petrology 130, 103–120.

Carter, B.A., 1987. The San Gabriel anorthosite–syenite–gabbro body, San Gabriel Mountains, California. In: Hill, M. (Ed.), Cordillera Section of the Geological Society of America, Centennial Field Guide, pp. 203–206.

Elvevold, S., Gilotti, J.A., 2000. Pressure–temperature evolution of retrogressed kyanite-eclogites, Weinschenk Island, North-East Greenland Caledonides. Lithos 53, 127–147.

Fisher, G.W., 1973. Nonequilibrium thermodynamics as a model for diffusion — controlled metamorphic processes. American Journal of Science 273, 897–924.

Fisher, G.W., 1977. Nonequilibrium thermodynamics in metamorphism. In: Fraser, D.G. (Ed.), Thermodynamics in Geology, pp. 381–403.

Fisher, G.W., 1978. Rate laws in metamorphism. Geochimica et Cosmochimica Acta 42 (7), 1035–1050.

Fisher, G.W., Lasaga, A.C., 1981. Irreversible thermodynamics in petrology. Reviews in Mineralogy 8, 171–209.

Foster, C.T., 1990. Control of material transportation and reaction mechanism by metastable mineral assemblage; an example involving kyanite, sillimanite, muscovite and quartz. Special Publications — Geochemical Society 2, 121–132.

Gilotti, J.A., 1993. Discovery of a medium-temperature eclogite province in the Caledonides of North-East Greenland. Geology 21, 523–526.

Gilotti, J.A., 1994. Eclogites and related high-pressure rocks from North-East Greenland. Rapport Grønlands Geologiske Undersøgelse 162, 77–90.

Gilotti, J.A., Elvevold, S., 1995. Eclogites and related high-pressure rocks in the Jøkelbugten region, North-East Greenland. In: Higgins, A.K. (Ed.), Express Report Eastern North Greenland and North-East Greenland 1995. Geological Survey of Greenland, Copenhagen, Denmark, pp. 43–52.

Gilotti, J.A., Elvevold, S., 1998. Partial eclogitization of the Ambolten gabbro-norite, North-East Greenland Caledonides. Schweizerische Mineralogische Und Petrographische Mitteilungen 78, 273–292.

Gilotti, J.A., Ravna, E.J.K., 2002. First Evidence for ultrahigh-pressure metamorphism in the North-East Greenland Caledonides. Geology 30 (6), 551–554.

Gilotti, J.A., Nutman, A.P., Brueckner, H.K., 2004. Devonian to Carboniferous collision in the Greenland Caledonides: U–Pb zircon and Sm–Nd ages of high-pressure and ultrahigh-pressure metamorphism. Contribution to Mineralogy and Petrology 148, 216–235.

Goldsmith, J.R., 1982. Plagioclase stability at elevated temperatures and pressures. American Mineralogist 66, 1183–1188.

Grant, J.A., 1986. The isocon diagram — a simple solution to Gresens' equation for metasomatic alteration. Economic Geology 81, 1976–1982.

Griffin, W.L., Heier, K.S., 1973. Petrological implications of some corona structures. Lithos 6, 315–335.

Holdsworth, R.E., Strachan, R.A., 1991. Interlinked system of ductile strike-slip and thrusting formed by Caledonian sinistral transpression in northeastern Greenland. Geology 19, 510–513.

Hull, J.M., Gilotti, J.A., 1994. The Germania Land deformation zone, North-East Greenland. Rapport Grønlands Geologiske Undersøgelse 162, 113–127.

Hull, J.M., Friderichsen, J.D., Gilotti, J.A., Henriksen, N., Higgins, A.K., Kalsbeek, F., 1994. Gneiss complex of the Skaerfjorden region (76^0–78^0 N), North-East Greenland. Rapport Grønlands Geologiske Undersøgelse 162, 35–51.

Indares, A., 1993. Eclogitized gabbros from the eastern Grenville Province: textures, metamorphic context, and implications. Canadian Journal of Earth Sciences 30, 159–173.

Indares, A., Dunning, G.R., 1997. Coronitic metagabbro and eclogite from the Grenville Province of western Quebec; interpretation of U–Pb geochronology and metamorphism. Canadian Journal of Earth Sciences 34 (7), 891–901.

Joesten, R., 1977. Evolution of mineral assemblage zoning in diffusion metasomatism. Geochimica et Cosmochimica Acta 41, 649–670.

Joesten, R., Fisher, G.W., 1988. Kinetics of diffusion controlled mineral growth in the Christmas Mountains (Texas) contact aureole. Geological Society of America Bulletin 100, 714–732.

Johnson, C.D., Carlson, W.D., 1990. The origin of olivine–plagioclase coronas in metagabbros from the Adirondak Mountains, New York. Journal of Metamorphic Geology 8, 697–717.

Kalsbeek, F., 1995. Geochemistry, tectonic setting, and poly-orogenic history of Paleoproterozoic basement rocks from the Caledonian fold belt of the North-East Greenland. Precambrian Research 72 (3–4), 301–315.

Kalsbeek, F., Nutman, A.P., Taylor, P.N., 1993. Paleoproterozoic basement province in the Caledonian fold belt of North-East Greenland. Precambrian Research 63, 163–178.

Lang, H.M., Gilotti, J.A., 2001. Plagioclase replacement textures in partially eclogitized gabbros from the Sanddal mafic–ultramafic complex, Greenland Caledonides. Journal of Metamorphic Geology 19, 495–515.

Leake, B.E., Woolley, A.R., Arps, C.E.S., Birch, W.D., Gilbert, M.C., Grice, J.D., Hawthorne, F.C., Kato, A., Kisch, H.J., Krivovichev, V.G., Linthout, K., Laird, J., Mandarino, J.A., Maresch, W.V., Rock, N.M.S., Schumacher, J.C., Smith, D.C., Stephenson, N.C.N., Ungaretti, L.E.H., Whittaker, E.J.W., Youzhi, G., 1997. Nomenclature of amphiboles: report of the subcommittee on amphiboles of the International Mineralogical Association, Commission on New Minerals and Mineral Names. American Mineralogy 82, 1019–1037.

Markl, G., Foster, C.T., Bucher, K., 1998. Diffusion controlled olivine corona textures in granitic rocks from Lofoten, Norway: calculation of Onsager diffusion coefficients, thermodynamic modeling and petrological implications. Journal of Metamorphic Geology 16, 607–623.

McClelland, W.C., Power, S.E., Gilotti, J.A., Mazdab, F.K., Wopenka, B., 2006. U–Pb SHRIMP geochronology and trace element geochemistry of coesite-bearing zircons, North-East Greenland Caledonides. In: Hacker, B., McClelland, W.C., Liou, J.G. (Eds.), Ultrahigh-Pressure Metamorphism: Deep Continental Subduction. Geological Society of America Special Paper, vol. 403, pp. 23–43.

Mongkoltip, P., Ashworth, J.R., 1983. Quantitative estimation of an open-system symplectitic forming reaction: restricted diffusion of aluminum and silicon in coronas around olivine. Journal of Petrology 24, 635–661.

Morimoto, N., Fabries, J., Ferguson, A.K., Ginzburg, I.V., Ross, M., Seifert, F.A., Zussman, J., Aoki, K., Gottardi, G., 1988. Nomenclature of pyroxenes. Mineralogical Magazine 52, 535–550.

Mørk, M.B., 1985a. A gabbro to eclogite transition on Flemsøy, Sunmøre, western Norway. Chemical Geology 50, 283–310.

Mørk, M.B., 1985b. Incomplete high P–T metamorphic transitions within the Kvamsøy pyroxenite complex, west Norway: a case study of disequilibrium. Journal of Metamorphic Geology 3, 245–264.

Mørk, M.B., 1986. Coronite and eclogite formation in olivine gabbro (Western Norway): reaction paths and garnet zoning. Mineralogical Magazine 50, 417–426.

Pognante, U., 1985. Coronitic reactions and ductile shear zones in eclogitized ophiolite metagabbro, Western Alps, North Italy. Chemical Geology 50, 99–109.

Rivers, T., Mengel, F.C., 1988. Contrasting assemblages and petrogenetic evolution of corona and noncorona gabbros in the Grenville Province of western Labrador. Canadian Journal of Earth Sciences 25, 1629–1648.

Spear, F.S., 1993. Metamorphic phase equilibria and pressure–temperature–time paths. Mineralogical Society of America, Monograph Series.

Stecher, O., Henriksen, N., 1994. Sm–Nd model age of an early Proterozoic gabbro-anorthosite from the Caledonian fold belt in North-East Greenland. Rapport Grønlands Geologiske Undersøgelse 162, 135–137.

Wayte, G.J., Worden, R.H., Rubie, R.C., Droop, G.T.R., 1989. A TEM study of disequilibrium plagioclase breakdown at high pressure: the role of the infiltrating fluid. Contributions to Mineralogy and Petrology 101, 426–437.

Whitney, P.R., McLelland, J.M., 1973. Origin of coronas in metagabbros of Adirondack Mountains, New York. Contribution to Mineralogy and Petrology 39, 81–98.

Zhang, R.Y., Liou, J.G., 1997. Partial transformation of gabbro to coesite-bearing eclogite from Yangkou, the Sulu terrane, eastern China. Journal of Metamorphic Geology 15, 183–202.

Zharikov, V.A., Zaraisky, G.P., 1991. Experimental modeling of wall-rock metasomatism. In: Perchuk, L.L. (Ed.), Progress in Metamorphic and Magmatic Petrology. Cambridge University Press, pp. 197–245.